Response of the magnetotail to changes in the open flux content of the magnetosphere

S. E. Milan,[1] S. W. H. Cowley,[1] M. Lester,[1] D. M. Wright,[1] J. A. Slavin,[2] M. Fillingim,[3] C. W. Carlson,[3] and H. J. Singer[4]

Received 5 December 2003; revised 27 February 2004; accepted 10 March 2004; published 24 April 2004.

[1] We compare the open flux content of the magnetosphere, quantified by measurements of the size of the northern ionospheric polar cap, with the radius of the magnetotail at $X \approx -25\ R_E$, deduced from observations made by the IMP-8 spacecraft. During an 8-hour period of observation we estimate that the proportion of terrestrial flux that is interconnected with the solar wind varies between 12 and 2.5%. This latter extreme, representing an almost closed magnetosphere, follows the incidence of a solar wind dynamic pressure step, the onset of a large substorm, and a 3-hour period of northward IMF. The deflated and compressed magnetotail is predicted to have a radius as small as 12 R_E at this time. The magnetotail does not reinflate to more typical dimensions until some time after a southward turning of the IMF, leading to accumulation of open flux through low latitude reconnection. We compare our observations with estimates of the shape of the magnetopause from an empirical model. We also present a simple model of the varying length of the magnetotail, based on upstream solar wind conditions, and observations of the size of the polar cap. *INDEX TERMS:* 2744 Magnetospheric Physics: Magnetotail; 2740 Magnetospheric Physics: Magnetospheric configuration and dynamics; 2784 Magnetospheric Physics: Solar wind/magnetosphere interactions; 2776 Magnetospheric Physics: Polar cap phenomena; *KEYWORDS:* magnetosphere, magnetotail, solar-terrestrial coupling, substorms

Citation: Milan, S. E., S. W. H. Cowley, M. Lester, D. M. Wright, J. A. Slavin, M. Fillingim, C. W. Carlson, and H. J. Singer (2004), Response of the magnetotail to changes in the open flux content of the magnetosphere, *J. Geophys. Res.*, *109*, A04220, doi:10.1029/2003JA010350.

1. Introduction

[2] It has been demonstrated in several case examples [see *Milan et al.*, 2003, and references within] that changes in the area of the polar cap, defined here as that region of the ionosphere threaded by open field lines, are related to the occurrence of magnetic reconnection at the magnetopause or in the magnetotail. The ability to measure the area of the polar cap quantifies the amount of open flux in the magnetosphere and thereby allows the storage and release of magnetic energy within the system, tapped from the flow of the solar wind, to be monitored. This magnetic energy is stored through the formation of a magnetotail, and thus it is to be expected that the magnetotail should inflate and deflate in response to changes in polar cap area. It is the aim of the current paper to investigate this subject.

[3] The magnetospheric cavity forms within the solar wind as the antisunward flowing plasma is deflected by the impenetrable obstacle presented by the Earth's magnetic field (see Figure 1). This field is compressed until the elevated magnetic pressure balances the stress exerted normal to the magnetospheric boundary, the magnetopause, by the ram or dynamic pressure P_{dyn} of the solar wind [*Chapman and Ferraro*, 1931; *Mead and Beard*, 1964]. Under typical solar wind conditions the subsolar magnetopause stand-off distance is close to 10 R_E. Tangential stresses applied to the magnetopause pull the Earth's field into a long magnetotail. *Dungey* [1961] proposed that these tangential stresses arose as a consequence of magnetic reconnection between the Earth's field and the interplanetary magnetic field (IMF) embedded within the solar wind (near point A in Figure 1). This results in a proportion of terrestrial field lines which interconnect across the magnetopause with the IMF (points C in Figure 1) and which are then stretched by the flow of the solar wind. *Dungey* [1965] estimated that field lines remained linked to the solar wind, or "open," for approximately 4 hours before being closed by magnetic reconnection in the magnetotail (at point B), resulting in a tail some 1000 R_E in length. This tail flares slightly, from a radial dimension of $\sim$15 R_E near the Earth to perhaps $\sim$30 R_E some distance down-tail, such that the component of the solar wind dynamic pressure acting normal to the magnetopause ($2P_{\mathrm{dyn}} \cos^2 \xi$ for specular reflection of the solar wind from the boundary) balances the internal magnetic pressure [e.g., *Caan et al.*, 1973;

[1]Department of Physics and Astronomy, University of Leicester, Leicester, UK.
[2]NASA Goddard Space Flight Center, Greenbelt, Maryland, USA.
[3]Space Science Laboratory, University of California, Berkeley, California, USA.
[4]Space Environment Center, Boulder, Colorado, USA.

Copyright 2004 by the American Geophysical Union.
0148-0227/04/2003JA010350$09.00

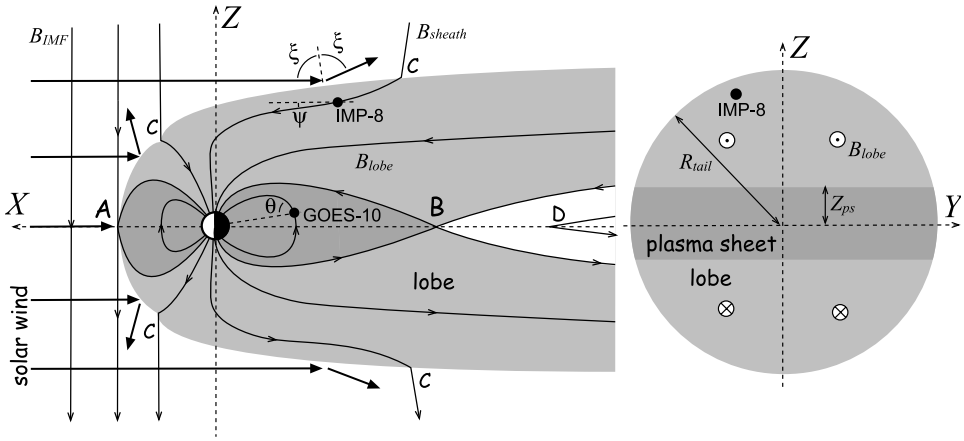

Figure 1. A schematic of the magnetosphere in the GSE *X-Z* and *Y-Z* planes. The light grey shading indicates the region of open flux, and dark grey indicates the closed flux region; no shading indicates regions where magnetic field lines belong entirely to the IMF, that is, are disconnected from the Earth. Also shown are the magnetic field angles ψ and θ, and the angle of incidence of the magnetosheath flow on the flared magnetopause ξ (see text for details).

Petrinec and Russell, 1996]. *Coroniti and Kennel* [1972] estimated that beyond $X \sim -150\ R_E$ the tail is of uniform radius, the normal stress on the magnetopause being determined entirely by the isotropic solar wind thermal and magnetic pressures. These calculations suggest that the magnetic field strength within the magnetotail necessary to balance the external forces is approximately 20 nT in the near-Earth tail, dropping to 9 nT in the distant tail. These estimates of magnetotail dimension and field strength have subsequently been borne out by studies with IMP-6 and ISEE-3 magnetic data (e.g., *Slavin et al.* [1985]; also see reviews of *Ness* [1987] and *Fairfield* [1987]).

[4] The cross-sectional area of the tail and its internal magnetic field strength are clearly also determined by the amount of open flux contained within the magnetosphere (see, for example, *Unti and Atkinson* [1968] and review of *Russell and McPherron* [1973]). The magnetotail comprises two back-to-back D-shaped regions of open flux, the magnetotail lobes which map to the northern and southern ionospheric polar caps, sandwiched between which is the plasma sheet (Figure 1). As the amount of open flux in the system waxes and wanes, the tail should inflate and deflate in concert [e.g., *Unti and Atkinson*, 1968; *Holzer and Slavin*, 1979]. *Caan et al.* [1975] found that the magnetic energy density within the tail increased during substorm growth phase and was subsequently released during the substorm expansion phase. This was also examined by *Fairfield* [1986], who noted that spacecraft in both the near-Earth magnetotail [*Maezawa*, 1975] and distant magnetotail [*Baker et al.*, 1984] had been observed to move into and out of the tail in response to substorm growth and expansion phase, respectively. This was interpreted by Fairfield as the tail inflating in response to the accumulation of open flux in the magnetosphere and correspondingly deflating at the onset of reconnection in the tail. In this study we take this theme further by examining the motion of the IMP-8 spacecraft relative to the tail magnetopause and correlate this with a measurement of the quantity of open flux in the system.

[5] We concentrate on an interval that has previously been studied to determine the dayside auroral and convection dynamics in response to northward IMF and high-latitude reconnection [*Milan et al.*, 2000a] and southward IMF and low-latitude reconnection [*Milan et al.*, 2000b]. Here we investigate changes in the area of the polar cap throughout the interval and show how changes in the open flux content of the magnetosphere affect the configuration of the magnetotail. It is found that following the incidence of a solar wind shock wave on the magnetosphere, a large substorm leads to a dramatic reduction in the area of the polar cap and the magnetotail appears to deflate. The magnetotail subsequently reinflates after the onset of dayside low-latitude reconnection in response to a southward turning of the IMF. We compare our estimates of magnetotail dimension with the empirical model presented by *Shue et al.* [1998], which is parameterized by the upstream solar wind dynamic pressure and the north-south B_z component of the IMF.

2. Observations

[6] The period of observation covers approximately 0400–2400 UT, 26 August 1998 (day 238), though we concentrate in detail on the interval 0400–1230 UT, when ionospheric observations allow the size of the polar cap to be quantified. Several spacecraft are employed to monitor the state of the magnetosphere during this interval. Figure 2 provides an overview of the spacecraft orbits between 0400 and 2400 UT, in the GSE X-Z and X-Y planes, dots indicating their locations at 1000 UT. Far upstream of the Earth, ACE and Wind provide information regarding the approaching solar wind and IMF conditions. Geotail, just upstream of the bow shock, gives independent confirmation of the solar wind propagation delay. The UV imager onboard the Polar spacecraft captures images of the northern hemisphere auroral configuration, from which the area of the polar cap can be estimated, aided by measurements of precipitating particles at low altitudes from the FAST spacecraft. Being located near the northern lobe magnetopause down-tail at $X \approx -25\ R_E$, the IMP-8 spacecraft

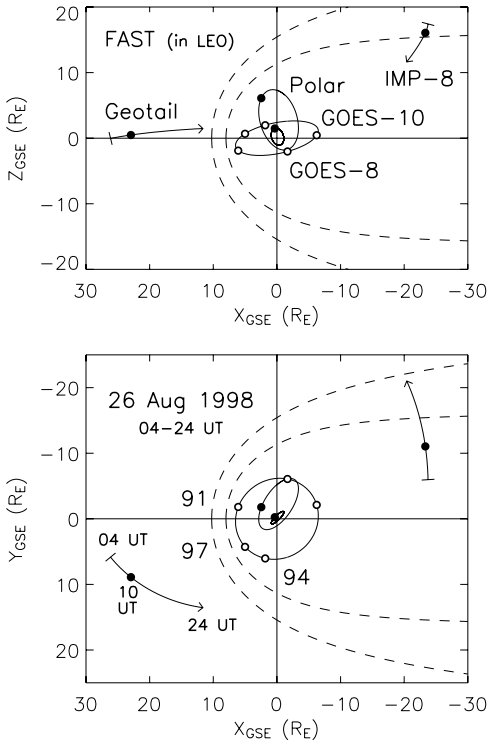

Figure 2. The locations in the GSE *X*-*Z* and *X*-*Y* planes of the spacecraft employed in this study. For clarity geosynchronous satellites are indicated by open circles, and other spacecraft are indicated by filled circles. Here 91, 94, and 97 refer to LANL 1991-080, 1994-084, and 97A, respectively.

moves into and out of the magnetosphere in response to changes in the configuration of the magnetotail, while the GOES-8 and -10 and LANL 1991-080, 1994-084, and 97A satellites monitor the magnetic field and particle response at geosynchronous orbit. During our interval the solar wind dynamic pressure varies considerably and the location of the magnetopause is expected to change accordingly. Superimposed by dashed lines are predictions of the magnetopause location when the magnetosphere is at its least (prior to 0700 UT) and most (∼0730 UT) compressed, based on the model of *Shue et al.* [1998]. The magnetopause location is expected to pass over the position of IMP-8, but other near-Earth spacecraft are contained within the magnetosphere at all times. We now present the observations from each spacecraft in turn. From here on in, spacecraft locations are described in GSE coordinates and magnetic field components in GSM coordinates.

2.1. Solar Wind and IMF: ACE, Wind, and Geotail

[7] Wind and ACE are located at $X \approx 120\ R_E$ and 248 R_E, respectively, both within 25–30 R_E of the Sun-Earth line. Geotail is located just upstream of the Earth's bowshock, near $X \approx 20\ R_E$. Allowing for the propagation delay of the solar wind, comparison of the solar wind and IMF parameters measured by these three spacecraft indicate an extremely close correspondence between the observations, despite the distance between them. Ideally, the Geotail measurements would be used to characterize the incoming solar wind, but large gaps in this data-set mean that we concentrate instead on the Wind observations, shown in Figure 3. The three components of the IMF are shown in Figures 3a–3c in GSM coordinates, with solar wind speed V_{SW} and number density N_{SW}, ion and electron temperatures T_i and T_e, and the solar wind dynamic pressure $P_{\rm dyn} = m_p N_{SW} V_{SW}^2$ (where m_p is the proton mass, and we have included a 5% contribution from He), indicated below in Figures 3d–3g, respectively. Of most interest to this study is the sharp increase in $P_{\rm dyn}$ from 2 to 12 nPa seen near 0640 UT and the subsequent return to more quiescent conditions in the following hours. The solar wind speed associated with the shock front is 600 km s^{-1}, which would usually lead to an estimated propagation delay between observations at Wind and arrival at the magnetopause of

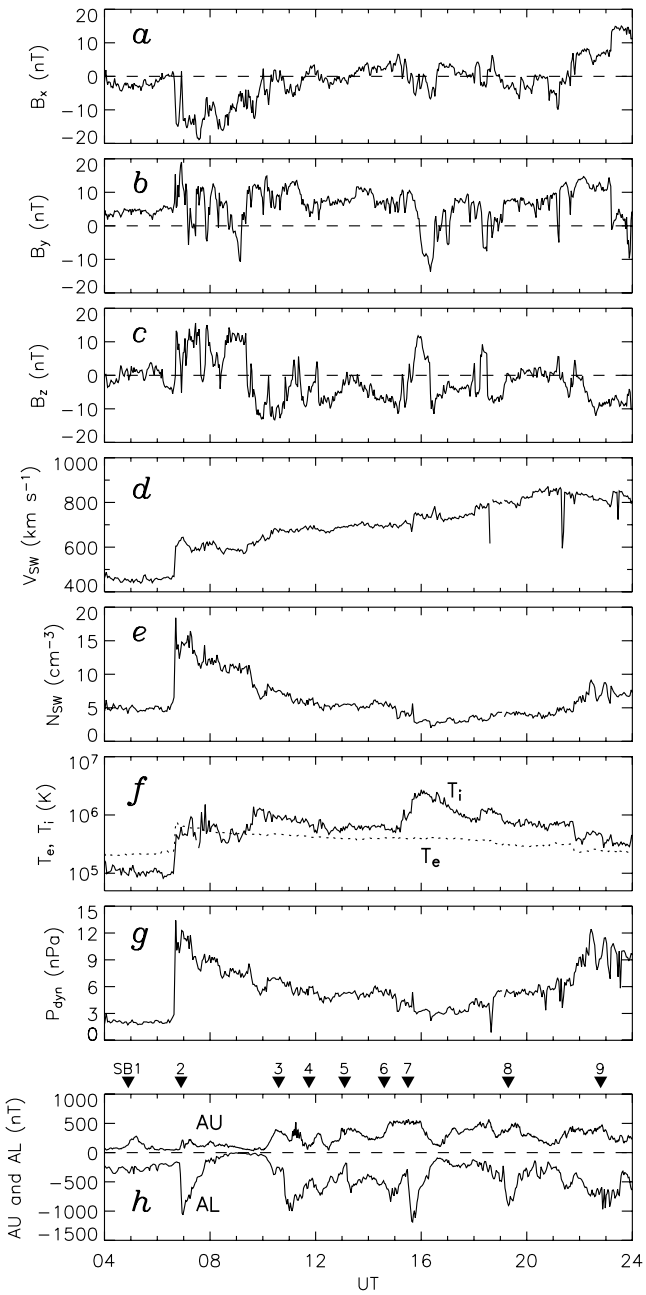

Figure 3. IMF field components, solar wind speed, and solar wind dynamic pressure, observed by the Wind spacecraft.

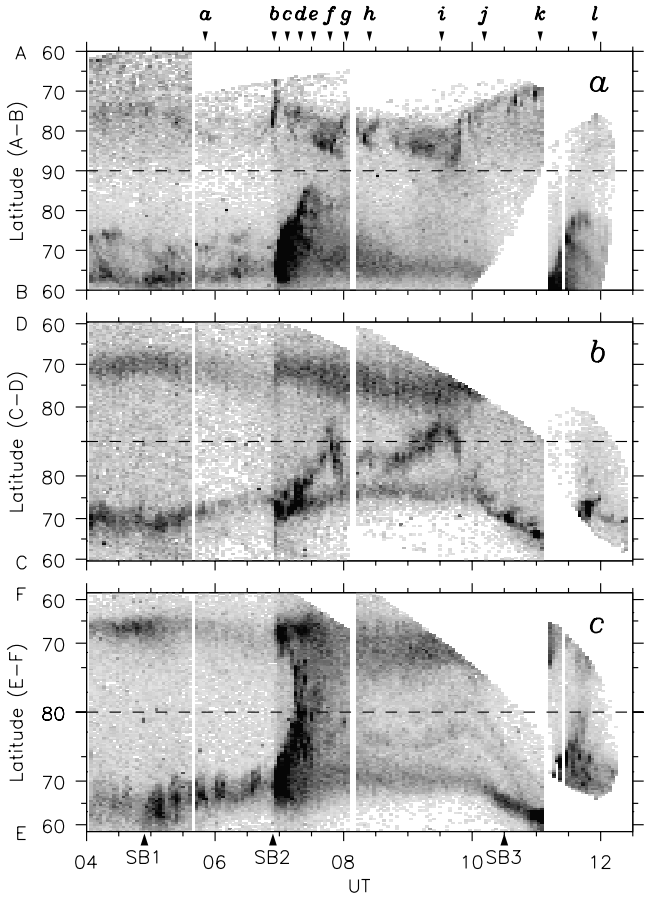

Figure 4. (a–c) Auroral luminosity as a function of time along three meridians indicated in Figure 5b, as observed by Polar UVI. Latitudes are geomagnetic. Darker shading indicates brighter aurora.

some 20 min. However, the shock front is clearly traveling faster than this, and Geotail observations suggest a delay of 10–15 min. The arrival of the shock front at the magnetosphere near 0655 UT marks the onset of a geomagnetic storm, identified by the characteristic initial, main, and recovery phases in D_{st} [*Matsushita*, 1967]. The storm has a two-stage onset, the initial phase occurring at the shock arrival, D_{st} reaching a first minimum of −50 nT at 2100 UT, before the full main phase (−155 nT) on the following day. Following the shock front the IMF is directed strongly northward ($B_z \approx +10$ nT) for 3 hours. The auroral dynamics observed during this 3-hour interval have previously been reported by *Milan et al.* [2000a]. Subsequently, the IMF turns strongly southward ($B_z \approx -10$ nT), first arriving at the magnetosphere at around 0950 UT; the auroral dynamics observed at this time formed the basis of studies by *Milan et al.* [2000b] and *Lockwood et al.* [2001]. The interested reader is directed to these three papers for a more detailed description of the small-scale dynamics observed at these times.

2.2. Polar Ionosphere: Polar UVI and FAST

[8] As indicated above, the arrival of the shock front in the solar wind heralds an interval of enhanced geomagnetic activity. Figure 3h shows the variation of the AL and AU geomagnetic indices for the period in question; the AE index is given by the difference between AU and AL [*Davis and Sugiura*, 1966]. The characteristic signatures of several substorms can be discerned, the expansion phase onsets being indicated by arrows. We refer to these as substorm breakups 1 to 9 (SB1–SB9). Perhaps the AL/AU signatures of some of the breakups we have identified are not that clear; observations shown later will strengthen the case for these. Of most interest to the present study are SB1, 2, and 3, as these occur when UV images are available, though many of the others will be shown to have a direct impact on the configuration of the magnetotail also. SB1 to 3 occur at approximately 0455, 0655, and 1030 UT, respectively. SB1 has a relatively small peak in AE of 500 nT, though SB2 and SB3 have larger peak values of 1300 and 1200 nT, respectively.

[9] The Ultraviolet Instrument (UVI) onboard Polar [*Torr et al.*, 1995] provides images of the northern hemisphere auroral configuration from before the arrival of the shock front until approximately 1220 UT. Figure 4 shows the time-sequence of auroral luminosity in the LBHs band along the noon-midnight magnetic meridian A–B (a) and two cuts from dusk to dawn C–D (b) and E–F (c), for the interval 0400–1230 UT (these meridians are indicated in Figure 5b). Several times are marked on Figure 4a, corresponding to the auroral images shown in Figures 5a–5l in a magnetic latitude and MLT frame. Concentric circles in Figure 5b mark magnetic latitudes of 60°, 70°, and 80°, and magnetic noon is located at the top of each panel. We show two dawn-dusk meridians, as Figure 4b allows the dynamics of the dayside aurora to be investigated, whereas Figure 4c focuses on the nightside phenomena, such as the substorm auroral bulge.

[10] A brightening of the nightside auroral oval at 0455 UT (Figure 4c) marks the onset of the first substorm SB1, though the auroral effects of this are relatively minor. The most spectacular dynamics occur after the arrival of the solar wind shock front. Prior to the arrival of the shock the auroral oval is relatively dim (Figure 5a). The first visible sign of the incidence of the shock, a brightening of the dayside auroral oval, is observed at 0652 UT. This is accompanied by a short-lived auroral brightening at post-noon midlatitudes (0655 UT, Figure 5b), known as a dayside detached aurora, a recognized signature of sudden solar wind dynamic pressure enhancements and northward IMF [see *Zhang et al.*, 2003, and references therein]. At the same time, the nightside, especially premidnight, oval brightens considerably, and a large auroral substorm (SB2) commences. The substorm bulge progresses polewards over the next half hour (Figures 5c–5e), reaching almost to the geomagnetic pole along the noon-midnight meridian (Figure 4a). By 0747 UT (Figure 5f), most of the polar region is covered by auroral luminosity. Following this, the bulge luminosity fades (Figures 5f–5i), to leave a faint nightside auroral oval with its poleward edge near 70° latitude, close to its original location prior to the storm onset (Figure 4a). As the substorm bulge fades after 0730 UT, two transpolar arcs become apparent, especially after 0830 UT and most clearly seen in Figure 5i. The presence of these transpolar arcs indicates that at least some of the polar region comprises closed field lines [e.g., *Henderson et al.*, 1996].

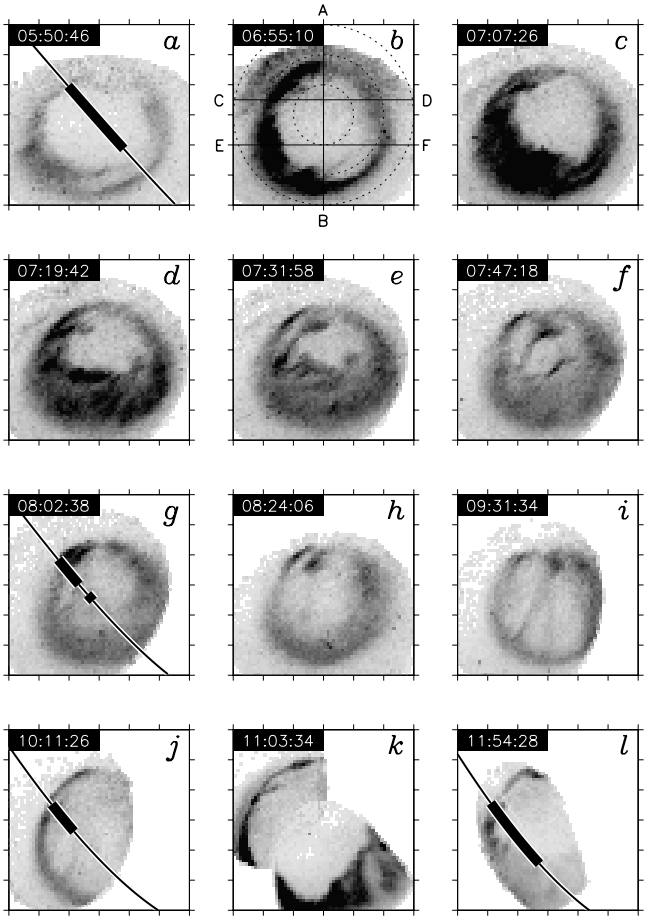

Figure 5. Snapshots of auroral luminosity presented in a magnetic latitude and local time frame, observed by Polar UVI at selected times during the interval of interest. Figure 5b indicates the three meridians of Figure 4 and the locii of magnetic latitudes 60°, 70°, and 80°; local noon is at the top of each panel. The ground track of the FAST spacecraft is indicated in four panels, the thicker bar indicating the presence of open field lines.

[11] Throughout this period (0700–0950 UT, Figures 5b–5i), the noon sector oval shows considerable and dynamic variations in brightness, though with an overall trend of poleward motion from near 75° to 85° latitude (Figure 4a). At the same time the dawn and dusk sector auroral zones are seen to progress polewards from 73° to 77° latitude (Figure 4b). The short time-scale variations in the luminosity are associated with an auroral spot located just poleward of the noon auroral oval (most obvious in Figures 5h and 5i), associated with the northward IMF cusp [*Milan et al.*, 2000a; *Fuselier et al.*, 2002; *Frey et al.*, 2003].

[12] After 0950 UT the IMF turns southward. The auroral oval progresses rapidly to lower latitudes, from 85° to 70° latitude along the noon meridian (Figure 4a) and from 75° to 65° along the dusk meridian (Figure 4b) by 1050 UT. Small-scale auroral dynamics observed in the noon and dusk sectors during this period are consistent with episodic, low-latitude merging [*Milan et al.*, 2000b; *Lockwood et al.*, 2001]. Unfortunately, the overall response of the midnight and dawn sector ovals to the southward turning of the IMF cannot be determined, as the field-of-view of the UVI camera diminishes in size as Polar moves away from apogee. We reasonably assume, however, that the auroral oval expands to lower latitudes at all local times. By 1103 UT (Figure 5k, a composite of two images taken just before and just after a repointing of the UVI camera), the oval has expanded to very low latitudes and another substorm breakup (SB3) has occurred. The poleward motion of the bulge can been seen in Figure 4a. It is clear from these observations that the open polar cap does not at this time decrease in size to the same extent as following the solar wind shock.

[13] The occurrence of substorm break-up indicates the onset of magnetic reconnection in the magnetotail, involving the closure of open flux. The substorm bulge delineates the ionospheric projection of the region of previously open lobe magnetic field lines that are closed by this reconnection. In Figure 5e it is clear that at least half of the open flux present before the onset of substorm SB2 is closed by 0730 UT. New open flux can be created by dayside reconnection at low latitudes, but this is not expected to occur when the IMF is directed northward, as it is until 0950 UT. Thus even though the substorm bulge diminishes in brightness such that most of the polar ionosphere appears largely devoid of auroras (e.g., Figure 5j), we suggest that much of this region is still closed. We employ four overpasses of the polar region by the FAST spacecraft to confirm this.

[14] Figure 6 shows spectrograms of precipitating ions and electrons from FAST overpasses of the northern hemisphere polar regions centered around 0545, 0800, 1010, and 1220 UT, each pass lasting some 30 min or so. The footprint of these overpasses are shown in Figures 5a, 5g, 5j, and 5l. In each case the FAST spacecraft progressed from the postnoon to the postmidnight sector, all four passes following a similar track. In the first overpass (Figure 5a), high fluxes of ~10 keV ions and electrons (0533–0535 UT and 0601–0606 UT) are indicative of trapped particles on closed field lines. More sporadic and lower energy (though >1 keV) ions and electrons on the nightside (0556–0601 UT) must also be present on closed field lines, as no mechanism is known for accelerating particles to such energies on open field lines. Similar energies on the dayside (0535–0537 UT), poleward of higher energy fluxes, are assumed to be present on open, though recently reconnected, field lines, particles being accelerated by the merging process. Figure 5 of *Milan et al.* [2003] indicates how such fluxes relate to the location of the merging gap and open/closed field line boundary for both northward and southward IMF. Regions devoid of ions and with only low energy (<300 eV) electrons, known as polar rain, are indicative of open field lines. In this case, then, the spacecraft traverses open field lines from 0535–0555 UT, indicated by the black bar at the top of Figure 6a and in bold on the satellite track of Figure 5a, corresponding to a relatively large polar cap. In sharp contrast, the second overpass (Figure 6b) encounters almost continual fluxes of high energy particles all the way across the polar region. Trapped particles are observed at the dayside crossing of the auroral zone (0746–0748 UT). Poleward of this (0748–0755 UT), fluxes are assumed to correspond to recently reconnected (high-

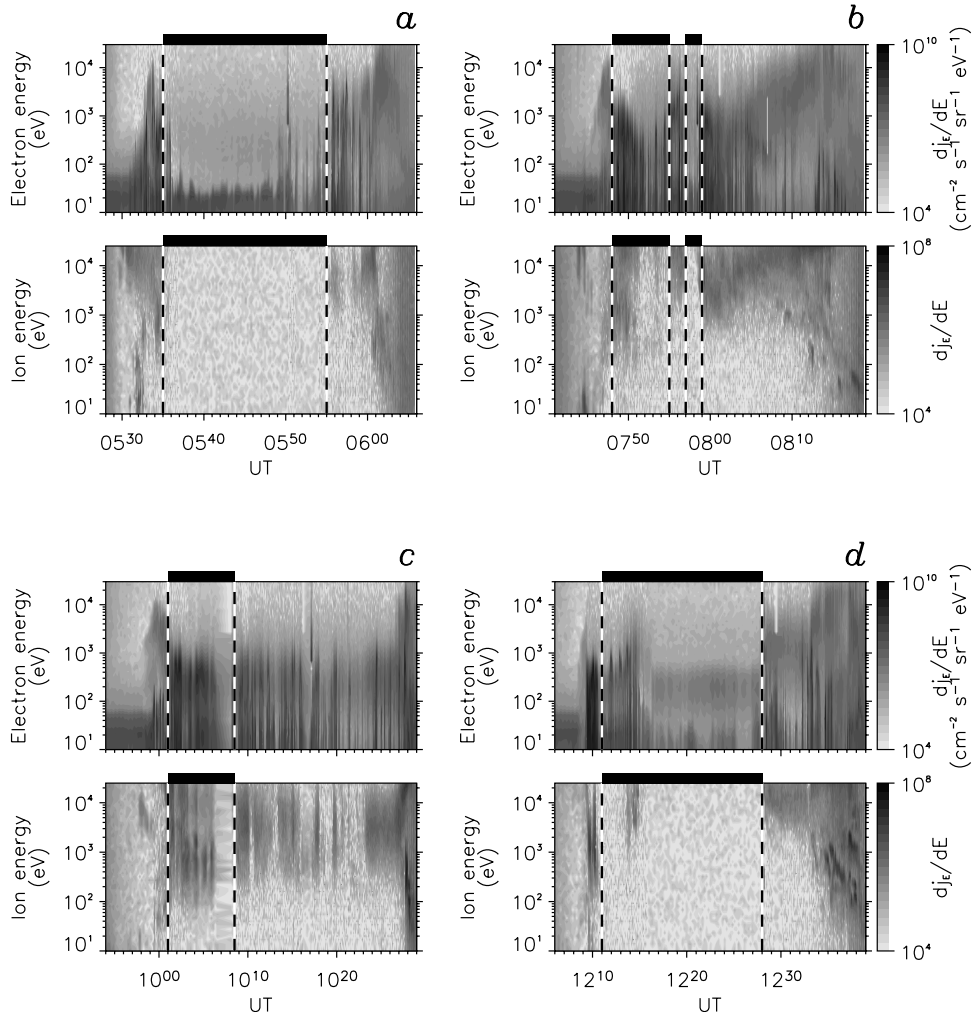

Figure 6. Electron and ion spectrograms from the four FAST overpasses. Vertical dashed lines and dark bars indicate the occurrence of particle fluxes consistent with open field lines.

latitude merging site) open field lines. Particle energies rise again (0755–0757 UT) as the spacecraft traverses a region of faint luminosity associated with the transpolar arcs (Figure 5g), presumably located on closed field lines. Following this is a very short interval of fluxes consistent with polar rain on open field lines (0757–0758 UT). The rest of the polar crossing indicates continual precipitation on closed field lines. Regions of open field lines are indicated in bold on the track overlaid on Figure 5g. The apparent coincidence of very bright aurora with open field lines is a consequence of a poleward motion of the dayside auroral oval during the ~30 min duration of the FAST overpass: at 0748 UT, when FAST crosses the dayside auroral zone, the bright aurora are located equatorward of the open field line region. More importantly, most of the nightside polar ionosphere is seen to project to closed field lines, despite auroral luminosities being very dim in this region.

[15] The third FAST overpass observes a similar particle environment to the second. The identification of precipitating fluxes consistent with open field lines is indicated in Figure 6c and Figure 5j. In other words, although low latitude reconnection has been ongoing for some 20 min by the time the spacecraft traverses the nightside polar regions, most of this region is still closed. By the time of the fourth overpass, however, FAST encounters polar rain, indicative of open field lines, along the majority of its track (Figure 6d), very similar to the first overpass. This track is superimposed on an auroral image taken just before the start of the overpass (Figure 5l), as after this time very little of the auroral oval is observed by UVI.

[16] We summarize these observations as follows. Prior to substorm breakup SB2 a large region of open flux is encompassed within the auroral oval. After the arrival of the shock front and the onset of substorm-related tail reconnection, the region of open flux contracts to less than half of its original size over a period of 30–40 min. At this time the IMF is directed northward, so no new open flux is created by dayside low-latitude reconnection. However, the luminosity within the nightside polar region diminishes, presumably as a consequence of a reduction of the precipitation from the plasma sheet. It is not until the southward turning of the IMF that low-latitude reconnection at the magnetopause creates new open flux and the auroral zone expands to lower latitudes to accommodate the increasing

size of the polar cap. In section 3.1 we determine the variation in open flux more quantitatively.

2.3. Magnetotail: IMP-8

[17] During the interval of interest the IMP-8 spacecraft is located near the northern lobe magnetopause, 25 R_E downtail of the Earth (see Figure 2). At the start of the interval the spacecraft is located within the magnetosphere, but as its trajectory carries it in the negative Y direction it is expected to make an outbound crossing of the magnetopause into the magnetosheath at some time during our period of observations. In fact, IMP-8 makes several crossings of the magnetopause as the magnetosphere is compressed and expands in response to changes in solar wind dynamic pressure and magnetotail configuration. It is the timing of these magnetopause crossings on which we now concentrate.

[18] Unfortunately, no IMP-8 plasma measurements are available at this time. However, Figures 7a–7d present magnetic field measurements from IMP-8 (B_x, B_y, B_z in GSM coordinates and total field magnitude B_T, respectively) from the period 0400–2400 UT. Superimposed are the Wind magnetic field measurements of the IMF, time lagged by 18 min to account for the propagation delay of the solar wind, indicated by dotted curves. At the start of the interval, B_x measured by IMP-8 has a value close to 20 nT and B_y and B_z are small. This orientation and field magnitude is consistent with the northern lobe, field lines being stretched antisunward but pointing towards the Earth to form the magnetotail (Figure 1). At approximately 0700 UT, the time of the arrival of the solar wind shock at the magnetosphere, the IMP-8 B_x component changes sign abruptly. For the next 3 1/2 hours the IMP-8 measurements closely resemble those of Wind, in direction if not magnitude, suggesting that IMP-8 has exited the magnetosphere and is sampling the magnetosheath field.

[19] Figure 7f shows the ratio of the total field strengths measured by IMP-8 and Wind, $r_B = B_T$ (IMP − 8)/B_T (Wind). At the start of the interval, IMP-8 is within the magnetosphere and r_B is close to 4, that is the magnetospheric field strength is much greater than that in the IMF. When IMP-8 enters the magnetosheath and hence measures a similar field to Wind, r_B drops to a value near 1.5. As this value is greater than unity, it indicates that the magnetosheath field is compressed with respect to the IMF. At approximately 1030 UT, B_x as measured by IMP-8 increases back to lobe values, at this time near 30 nT, indicating a reentry of the magnetosphere. At this time, r_B increases above 2 again as the magnetospheric field intensity is much greater than the IMF. Following this, there are subsequent outbound and inbound crossings of the magnetopause, at 1110, 1255, 1330, 1445, and 2130 UT; each crossing is indicated by a vertical dashed line. We employ the criterion that $r_B > 2$ to demarcate between intervals when IMP-8 is located within the magnetosphere and within the magnetosheath $r_B < 2$. This demarcation has been followed through to Figure 7h, which indicates the distance of IMP-8 from the GSE X-axis, the axis of symmetry of the magnetotail, or in other words $R^2 = Y^2 + Z^2$; this curve is plotted thick when the spacecraft is within the magnetosphere and thin when it is within the magnetosheath. R increases with time as IMP-8 moves to increasing Y along its orbit. In addition, the dotted line indicates the *Shue et al.* [1998] prediction of the

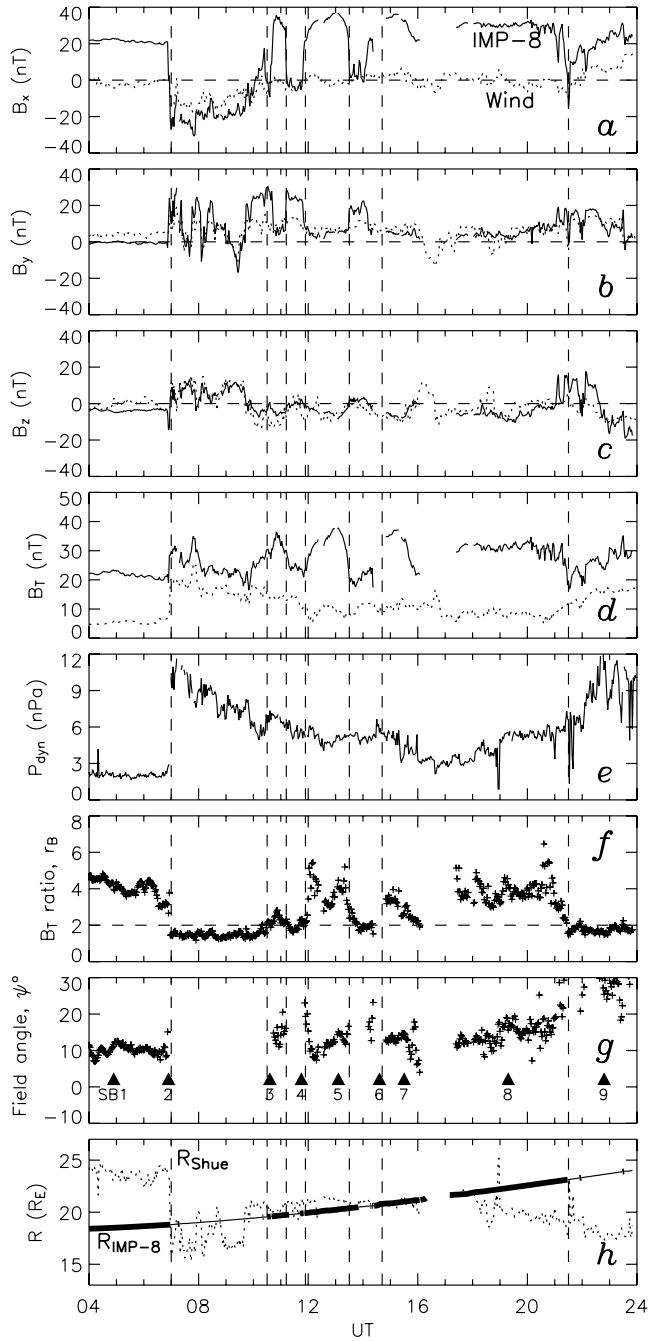

Figure 7. (a–d) Three magnetic field components and total field strength as measured by IMP-8 (full curves) and Wind (dashed curves). (e) The solar wind dynamic pressure measured by Wind. (f) The ratio of magnetic field strengths measured by Wind and IMP-8, r_B. (g) The angle of the IMP-8 field measurements to the sun-Earth line, which we term the field angle, ψ. (h) The radial location of IMP-8 from the X-axis, shown bold when the magnetic field observations suggest the spacecraft is within the magnetotail. Also shown is the radial dimension of the magnetotail predicted by the *Shue et al.* [1998] model (dotted curve).

radius of the magnetotail, at the X of IMP-8, parameterized by the upstream P_{dyn} and IMF B_z measurements made by Wind.

[20] At the start of the interval the radius of the magnetotail is predicted to be approximately 24 R_E, placing IMP-8 well inside the magnetosphere (this time interval corresponds to the least compressed magnetopause shown in Figure 2). Following the arrival of the solar wind shock the magnetosphere is expected to be compressed to within a radius of 16 R_E or so (the most compressed magnetopause in Figure 2) and IMP-8 exits into the magnetosheath as predicted. With the subsequent decline in $P_{\rm dyn}$, and especially the southward turning of the IMF, the magnetopause is predicted to expand over the spacecraft at 0950 UT. However, IMP-8 continues to make measurements consistent with the magnetosheath until 1030 UT. Thereafter, until about 1800 UT, there is some correspondence (within 1 R_E or so) between changes in predicted location of the magnetopause and entries or exits of the magnetosphere by IMP-8. After 1800 UT, although the magnetopause is predicted to be compressed within the location of IMP-8, the spacecraft remains in the lobe until 2130 UT. However, transient decreases in B_x and B_T measured by IMP-8 after 2000 UT indicate that the spacecraft is located very close inside the magnetopause at this time. It is the departure from predicted behavior at 0950–1030 UT that we concentrate on in this study.

[21] Before moving on, we note that the lobe field strength, measured when IMP-8 is within the magnetosphere, changes from near 20 nT at the start of the interval to 30 nT and above after 1000 UT. The increase in lobe field strength appears to correspond with the increase in $P_{\rm dyn}$ of the solar wind (Figure 7e), and this can easily be understood as a compression of the magnetotail until stress balance is achieved between an elevated magnetic pressure inside the tail $P_{\rm mag}$ and the magnetosheath dynamic pressure acting against the flared magnetopause. To demonstrate this, in Figure 8a we plot $P_{\rm dyn}$ (Wind) and $P_{\rm mag} = B_T^2/2\mu_0$ (IMP-8) together, though on different scales. A good qualitative fit is found between $P_{\rm dyn}$ and $P_{\rm mag}$ when IMP-8 is within the lobe, indicated by bars, except near magnetopause crossings when IMP-8 clearly traverses a boundary layer. A constant of proportionality close to 0.1 is found, i.e., $P_{\rm mag} \approx 0.1 P_{\rm dyn}$.

[22] As a check that this constant of proportionality is consistent with our expectations, we use the angle that the lobe magnetic field makes to the GSE X-axis, $\psi = \cos^{-1} B_x/B_T$, as a proxy for the flaring of the magnetotail (see Figure 1). As discussed in the Introduction, the normal stress applied to the magnetopause by the solar wind ram pressure should be close to $2P_{\rm dyn}\cos^2\xi$, so we expect that the constant of proportionality be close to $2\cos^2\xi \approx 2\cos^2(90^\circ - \psi)$. We show ψ in Figure 7g and find that it varies mainly between 8° and 15° when IMP-8 is in the lobe. We note that ψ tends to increase (the flaring increases) during substorm growth phases and to decrease following substorm onset, most obvious following SB1, 5, 7, and 8. This indicates that the flaring increases as open flux accumulates in the tail, and the flaring decreases as the tail deflates [cf. *Unti and Atkinson*, 1968]. Flaring angles of between 8° and 15° give values of $\cos^2\xi$ between 0.04 and 0.13, bracketing the 0.1 constant of proportionality found above. So far our analysis does not take into account the contributions of the magnetosheath gas and magnetic pressures to the normal stress on the magnetopause; these will be considered in section 3.2.

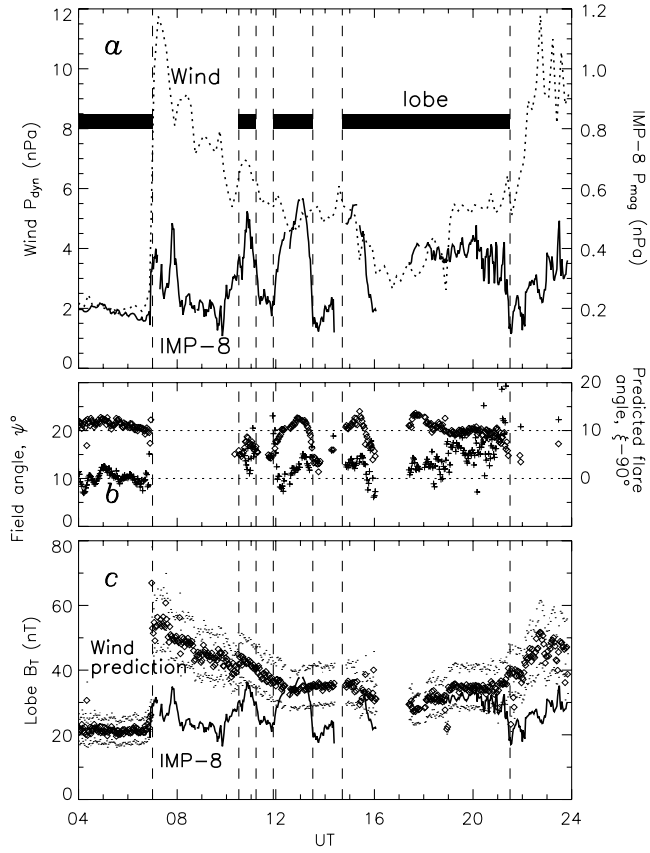

Figure 8. (a) The relationship between solar wind dynamic pressure observed by Wind and the magnetic pressure determined from the IMP-8 magnetic field measurement. Bars indicate when IMP-8 is located within the magnetotail. (b) A comparison between field angle ψ (crosses) and the predicted magnetotail flare angle 90°-ξ (diamonds); note that scales have been offset by 10° for clarity. (c) A prediction of the lobe field strength (diamonds) and compared with IMP-8 observations. Dots indicate variations in the predicted field strength for different assumed flaring angles of the magnetotail (see text for details).

2.4. Geosynchronous Orbit: GOES and LANL

[23] The GOES 8 and 10 satellites, situated at geosynchronous orbit, cross the noon-midnight meridian close to 0500 and 0900 UT, respectively. Both are located on the nightside during our interval of interest and so are ideally located to determine changes in the near-Earth magnetotail field structure associated with the arrival of the solar wind shock and in the subsequent hours. The GOES spacecraft measure magnetic field components known as H_p, H_e, and H_n, where H_p is perpendicular to the satellite orbital plane (parallel to the Earth's spin axis since the plane is very close to 0° inclination), H_e is perpendicular to H_p and directed earthward, and the third orthogonal component H_n points eastward. In this study we employ the angle of the magnetic field to the satellite-Earth line in the north-south meridian, that is $\theta = \tan^{-1} H_p/H_e$, to determine how dipolar or tail-like

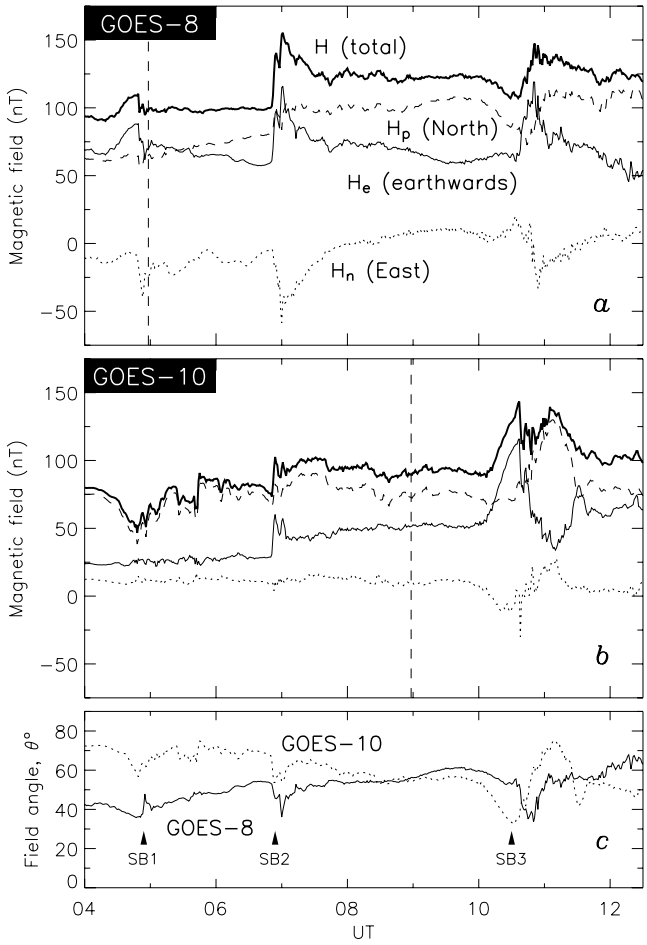

Figure 9. (a–b) Magnetic field measurements at geosynchronous orbit observed by GOES-8 and -10. Vertical dashed lines indicate the time at which each satellite crosses the midnight meridian. (c) The angle made by the field in the meridional plane.

the field is at $X \approx -6\ R_E$ (see Figure 1). Figure 9 shows the variation of the three magnetic field components, as well as the total field, (Figures 9a and 9b for GOES 8 and 10, respectively) and the variation of θ (Figure 9c) between 0400 and 1230 UT. The spacecraft are located at magnetic latitudes of $\Lambda = 10.8°$ and 4.4°, respectively, and consequently if the Earth's magnetic field was purely dipolar then θ would be close to 69° and 81° (as dip angle I is given by $\tan I = 2 \tan \Lambda$). In practice, on the dayside the magnetosphere is compressed so that θ tends to be greater than expected for a dipole, and on the nightside it is stretched into a magnetotail so that θ is less than expected.

[24] The first signatures of interest occur shortly after 0400 UT when θ decreases at both spacecraft, indicating the development of a more tail-like magnetic configuration, followed by an increase of θ after 0450 UT. This recovery towards more a more dipolar field structure, a "dipolarization," is a response to substorm onset SB1 and represents a disruption of the cross-tail current that is associated with the stretched field geometry and subsequent closure of open flux.

[25] At ~0650 UT, perturbations associated with the solar wind shock front are observed, mainly an increase in overall field strength as the magnetosphere is compressed, accompanied by a short-lived decrease in θ indicating a change to a more tail-like configuration. The θ recovers quickly, however, presumably as a response to substorm onset SB2 following the shock arrival. Thereafter θ remains relatively constant, slow changes probably reflecting local time variations in the field geometry, until ~0950 UT when θ decreases dramatically over the next 45 min, especially at GOES 10 which is nearest midnight. This is perhaps the most important aspect of the geosynchronous orbit observations, as it indicates that the tail configuration changes little during the interval of northward IMF following the shock front arrival, but after the southward turning the magnetosphere rapidly becomes more stretched and tail-like, reflecting an increase in open flux in the system and the development of the lobes. Shortly after 1030 UT, θ increases once again in response to substorm onset SB3.

[26] The LANL spacecraft 1991-080, 1994-084, and 97A also orbit at geosynchronous altitude at this time, making measurements of fluxes of protons and electrons in the energy ranges 50–400 keV and 50–315 keV, respectively (data not shown). These satellites are clustered on the dayside during the interval of interest, though all are able to detect significant increases in particle fluxes in response to substorm injections [e.g., *Arnoldy and Chan*, 1969; *McIlwain*, 1974] associated with SB1, SB2, and SB3; the last of these is also preceded by a drop-out of fluxes, which has previously been identified as a "plasma sheet thinning" [*Sauvaud and Winckler*, 1980] associated with an accumulation of open flux in the magnetosphere. Most importantly, however, there is no sign that these spacecraft exit the magnetosphere at any time. In other words, the near subsolar magnetopause remains outside geosynchronous orbit throughout this interval.

2.5. High-Altitude Cusp: Polar

[27] At the same time as recording images of the aurora, the Polar spacecraft is able to make in situ measurements of the plasma and magnetic field environment in the vicinity of the high-altitude cusp. In this study we concentrate on the field measurements alone. Figure 10 shows the total magnetic field magnitude measured by the Polar Magnetic Field Experiment (MFE) for the time interval 0400–1230 UT (Figure 10a, thick solid curve) along with the three GSM components (Figures 10b–10d). Superimposed as the thin curve is the Tsyganenko magnetic field model [*Tsyganenko*, 1995] estimation of the field components at the location of Polar; note the rapid increase in overall field strength after 1000 UT as the spacecraft moves to lower altitudes. In general, a good correspondence is found between the model and the observations, except during the interval between the vertical dashed lines (0655–0910 UT), from the arrival of the shock front and over the subsequent 2 hours. Here, marked departures from the model predictions are found, most notably perhaps the reversal of the sense of B_z, from negative to positive. This is difficult to understand if the spacecraft remains within the magnetosphere, as the field should point into the northern hemisphere. It seems reasonable to suggest then that the magnetopause is so compressed following the increase in solar wind dynamic pressure that Polar finds itself in the magnetosheath at this time. The dotted curves in Figure 10

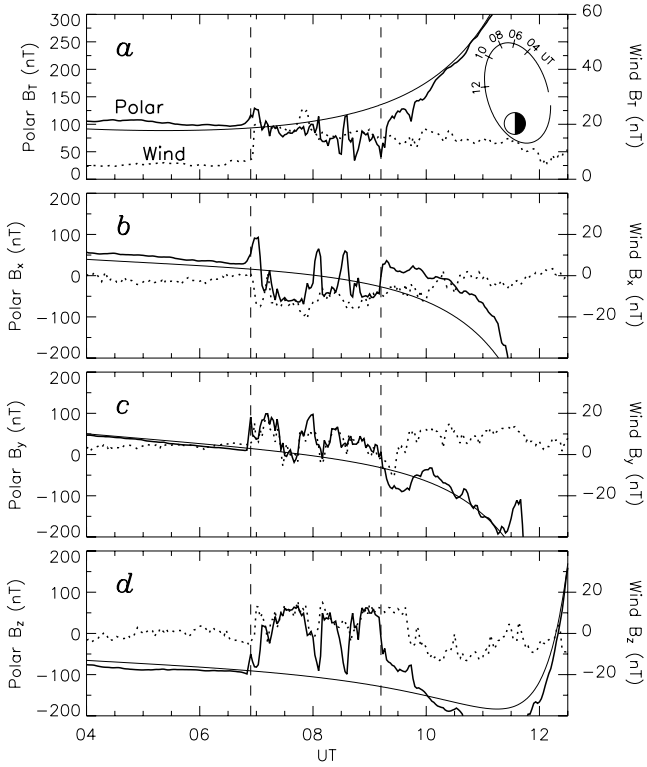

Figure 10. (a–d) Total magnetic field, and field components, measured at Polar (thick solid curves) and at Wind (dotted curves). Thin solid curves indicate predictions for the Polar observations from the T95 model. Vertical dashed lines indicate the interval during which significant departures from model expectation are observed. An inset figure shows the orbit of Polar in the X-Z plane (see also Figure 2).

show the Wind IMF observations, suitably time-lagged to the magnetosphere (note different scale). A very close match is found with the Polar observations during the dashed interval, confirming that this is indeed the case. *Lockwood et al.* [2001] examined the plasma environment of Polar during this interval and suggested that the observation of alpha particles and high-charge oxygen was also consistent with Polar being located in the magnetosheath at this time. The ratio of field strengths between Polar and Wind is close to 5, indicating that the magnetosheath field is compressed by this factor relative to the solar wind at this location, in a similar manner to the field ratio of 1.5 found down-tail at IMP-8 (see section 2.3). Shortly after 0900 UT the gradual decline in solar wind dynamic pressure, coupled with the decrease in altitude of Polar, results in a reentry of the magnetosphere. There are also possible transient reentries at 0805 and 0835 UT. These observations show that near $X \approx 0$ R_E the magnetosphere is compressed to within a radial distance $(Y^2 + Z^2)^{1/2} \approx 8$ R_E following the solar wind shock, well within the location predicted by the *Shue et al.* [1998] model.

3. Discussion

[28] Observations from a variety of spacecraft indicate that following a step in solar wind dynamic pressure to more than 10 nPa the magnetosphere becomes highly compressed, such that the Polar and IMP-8 spacecraft enter the magnetosheath. This indicates that the radius (actually, the cylindrical distance from the Sun-Earth line) of the magnetosphere and magnetotail near $X \approx 0$ and -25 R_E is less than 8 and 20 R_E, respectively. While the latter is consistent with the predicted location of the magnetopause in the *Shue et al.* [1998] model, the former is not, indicating a much smaller magnetosphere than expected. Geosynchronous orbit measurements from the LANL spacecraft show, however, that the subsolar magnetopause remains upstream of $X \approx 6.6$ R_E throughout the interval. Simultaneous observations of the northern hemisphere auroral dynamics show that a large substorm triggered by the shock arrival closes most of the open flux previously contained within the polar cap, suggesting a significant deflation of the magnetotail lobes. The IMF turns northwards at this time, so no reinflation of the lobes is expected until a southward turning of the IMF some 3 hours later. This might explain why IMP-8 does not reenter the magnetosphere until some time after the southward turning, despite a slackening of the solar wind dynamic pressure prior to this. In this section we determine changes in the open flux content of the magnetosphere and from these estimate the dimensions of the magnetotail.

3.1. Polar Cap Area

[29] Using the procedure described by *Milan et al.* [2003], we estimate the location of the open/closed field line boundary (OCB) at all local times from the Polar UVI, FAST, and SuperDARN observations; for brevity the latter are not presented in this paper, see instead *Milan et al.* [2000a, 2000b]. It is then a straightforward matter to integrate the radial component of the magnetic field (assumed dipolar) within this region to give the total open flux through the polar cap, F_{PC}. Figure 11a shows the time series of F_{PC} so determined. For simplicity, measurements are made only at key stages in the auroral evolution, marked by filled or open circles numbered 1–12, and F_{PC} is interpolated in between. For interest, we also mark the approximate voltages associated with the changes in flux, the difference between the day and nightside reconnection rates (cf. *Milan et al.* [2003], and see section 3.4). We note that the variation in F_{PC} can be recognized in the motion of the main regions of luminosity shown in Figures 4a–4c. The key stages in the auroral development are described below.

[30] (1) At the start of the interval the auroral oval appears rather quiescent, similar to that shown in Figure 5a. F_{PC} is found to be close to 0.55 GWb. (2) In the subsequent hour IMF B_z is small but negative (Figure 11b) and the auroral luminosity gradually moves to lower latitude as low-latitude reconnection at the magnetopause increases F_{PC} to 0.7 GWb. Stage 2 corresponds to the onset of the first substorm, SB1. (3) The onset of reconnection in the magnetotail associated with SB1 causes F_{PC} to decrease until stage 3, corresponding to the FAST overpass indicated in Figure 5a, and beyond until (4) just prior to the arrival of the solar wind shock; at this time $F_{PC} \approx 0.45$ GWb. The IMF is directed slightly northwards during most of this interval and no dayside low-latitude reconnection is expected, except for the last half hour, during which time there is a slight increase in F_{PC} to 0.5 GWb (Figure 5b).

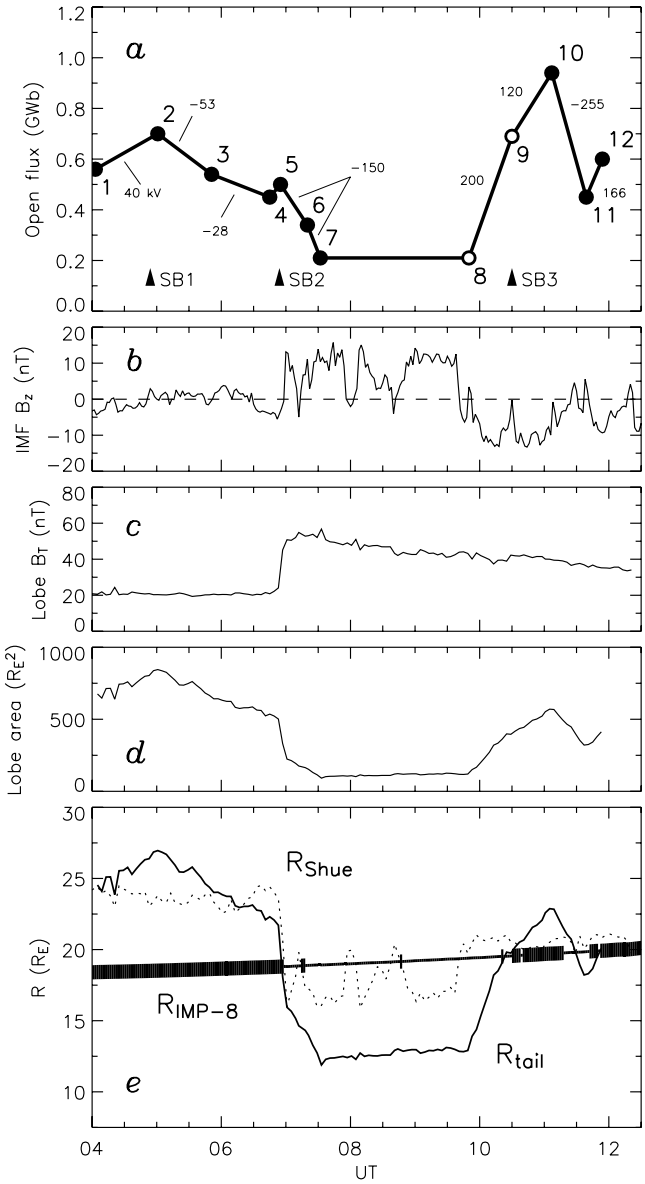

Figure 11. (a) An estimate of the open flux content of the magnetosphere from observations of the northern polar ionosphere. (b) The simultaneous IMF B_z observations from Wind. (c) An estimate of the magnetotail lobe magnetic field strength from the relationship with upstream solar wind dynamic pressure illustrated in Figure 7. (d) The corresponding cross-section area of each of the magnetotail lobes. (e) The expected radial dimension of the magnetotail (solid curve), the prediction of the *Shue et al.* [1998] model, and the radial position of IMP-8, shown thick when the spacecraft is within the magnetotail.

[31] (5) After the solar wind shock front arrives and substorm break-up SB2 commences, there is a rapid decrease in F_{PC} to as little as 0.2 GWb by 0730 UT (7) (see Figures 5c–5e). After this time it becomes more difficult to determine the size of the polar cap as the auroral luminosity at high latitudes fades, even though we know that much of this region is closed (Figures 5f–5i). At this point we must make some assumptions, and for this reason 8 and 9 are represented by open circles to indicate some uncertainty in F_{PC}. As the IMF is directed strongly northward from 0655 UT until the southward turning at 0950 UT, we assume that no additional opening of flux has taken place until (8), i.e., that $F_{PC} \approx 0.2$ GWb at this time. There is then a rapid equatorward motion of the auroral oval, indicating strong coupling with the IMF and the addition of significant amounts of open flux to the system.

[32] (9) The onset of substorm SB3 and the closure of flux in the magnetotail marks a slowing of the increase in flux within the polar cap. It is not stopped however, as open flux is continually being added on the dayside, as the IMF remains southwards. From Figure 5j it is clear that although the region of low luminosity within the auroral oval is very extended at this time, not all of this region maps to open flux. To estimate how much of this flux is open, we assume that at stage 8 $F_{PC} \approx 0.2$ GWb but that the total flux (open and closed) represented by the dim portion within the auroral oval at this time is estimated at close to 0.5 GWb (see for instance Figure 5i). The amount of closed flux at these high latitudes is then close to 0.3 GWb. During the subsequent expansion of the polar cap, we assume that this amount of dim closed flux remains constant until some time after the onset of SB3 (note the presence of transpolar arcs even after the southward turning of the IMF, section 2.2). Hence at stage 9 the amount of open flux is given by the flux enclosed by the bright auroral oval (0.95 GWb) minus this closed region, such that $F_{PC} \approx 0.65$ GWb.

[33] By stage 10, the polar cap has reached its maximum extent, $F_{PC} \approx 0.95$ GWb. At this time we assume that the reconfiguration of the magnetosphere by the substorm has resulted in all flux within the auroral oval being open, as confirmed by the FAST overpass shown in Figure 5l. By this time, the IMF is no longer strongly southward so dayside reconnection effectively ceases. Continued nightside reconnection associated with SB3 leads to a considerable reduction in open flux until stage 11, at which point $F_{PC} \approx 0.45$ GWb. The IMF turns southward once again, and there is an increase in F_{PC} to almost 0.6 GWb by stage 12, which represents the last usable images from Polar UVI.

[34] In summary, the open flux content varies by almost a factor of 5 during the interval of interest. As the total flux through each hemisphere of the Earth is close to 8 GWb, we estimate that at auroral stage 7 only 2.5% of the flux is open, whereas at stage 10 when the polar cap is at its greatest extent, this proportion has risen to 12%. Substorm SB2 is of interest as this is triggered by the arrival of a solar wind shock. *Petrinec and Russell* [1996] report three shock-triggered substorms during which the approximate amount of open flux closed is 0.4–0.5 GWb, whereas SB2 closes only 0.3 GWb. The discrepancy between these figures may be due to the small quantity of open flux remaining in the magnetosphere after SB2, 0.2 GWb, suggesting that it may be difficult to close all the open flux in the system. In the next section, we employ F_{PC} to estimate the dimensions of the magnetotail and compare this to the IMP-8 observations.

3.2. Cross-Sectional Area of the Magnetotail

[35] In cross section the magnetotail comprises two back-to-back D-shaped regions of open flux, the northern and southern lobes, sandwiching in between the plasma sheet, which is located on closed field lines earthward of the tail reconnection site and on "disconnected" IMF field lines

tailward of it (Figure 1). We assume that the overall cross-sectional area of the tail is twice that represented by an individual lobe, plus the cross-sectional area of the plasma sheet. The northern and southern lobes both contain an equal amount of flux and each map directly to the northern and southern ionospheric polar caps, respectively. If it is assumed that a negligible amount of flux crosses the magnetopause earthwards of IMP-8, we can equate the flux in each lobe at $X \approx -25\ R_E$ to F_{PC} determined from the ionospheric observations. The cross-sectional area of each lobe should then be

$$A_{\text{lobe}} = \frac{F_{PC}}{B_{\text{lobe}}}, \tag{1}$$

where B_{lobe} is the magnetic field strength within the lobes. IMP-8 cannot provide a continuous measure of B_{lobe} as the spacecraft moves in and out of the magnetosphere. However, in section 2.3 we noted that a relationship appeared to exist between solar wind dynamic pressure and magnetic pressure within the lobe, with a constant of proportionality close to 0.1 (see Figure 8a). If such a relationship can be shown to be reliable, then upstream Wind observations can be employed to estimate B_{lobe}, even when IMP-8 is not in the lobe.

[36] To this end, we turn to the full stress balance between the lobe magnetic pressure and the sum of solar wind dynamic, static and magnetic pressures (as, for example, *Petrinec and Russell* [1996], though here we have introduced a factor of 2 in the second term to properly account for specular reflection of particles from the magnetopause, not just incidence):

$$\frac{B_{\text{lobe}}^2}{2\mu_0} = 2P_{\text{dyn}} \cos^2 \xi + N_{SW} k_B (T_e + T_i) + \frac{B_{\text{IMF}}^2}{2\mu_0}, \tag{2}$$

where k_B and μ_0 have their usual meanings. In equation (2) we assume that the gas or static pressure in the lobe is negligible when compared with the magnetic pressure. Then, using measurements of B_{lobe} from IMP-8 when it is within the magnetotail, equation (2) can be used to estimate ξ, from which the flaring of the tail can be found. In Figure 8b we show $\xi - 90°$ (diamonds), to compare with the field angle ψ (crosses), which we used as a proxy for the magnetotail flare (note that the scales have been displaced by 10° for clarity, and horizontal dotted curves represent angles of 10°). A close match is found between these two estimates of the tail flare, with even variations with substorm phase being reproduced.

[37] Although a gratifying prediction of the flaring angle can be found, this is possible only when we have a knowledge of B_{lobe}. However, we want to use equation (2) to estimate B_{lobe}, even in the absence of actual tail measurements. In this case we must use a fixed value of ξ. We pick a value of $\xi = 79°$, corresponding to an 11° angle of flare, the approximate mean of ψ. Then Figure 8c shows the predicted value of B_{lobe}, along with the measurements of IMP-8, indicating a close correspondence when IMP-8 is within the magnetotail. We also show the predictions for $\xi = 79° \pm 2.5°$ (dots) to indicate how changes of flare with substorm phase might affect our estimates.

[38] This variation in B_{lobe} is reproduced, somewhat smoothed, in Figure 11c. Figure 11d then shows the estimated cross-sectional area of an individual lobe, found from equation (1). Following *Fairfield* [1986], we estimate the radius of the tail R_{tail} from

$$\pi R_{\text{tail}}^2 = 2A_{\text{lobe}} + 4R_{\text{tail}} Z_{PS}, \tag{3}$$

which equates the total cross-sectional area of the tail (left-hand side (LHS)) with that of the two lobes and a rectangular plasma sheet of half-thickness Z_{PS} (RHS), as indicated in Figure 1. Fairfield assumed that $Z_{PS} \approx 4$ and $3\ R_E$ at down-tail distances of $X \approx -60$ and $-200\ R_E$. We use a value of $Z_{PS} \approx 5\ R_E$ at $X \approx -25\ R_E$, though our results are not particularly sensitive to this parameter. From equation (3) it is trivial to find the expected magnetotail radius, which is shown in Figure 11e, along with the estimate from *Shue et al.* [1998]. Superimposed is the radial location of IMP-8, shown bold when the spacecraft is located within the magnetotail (see also Figure 7). There appears to be an excellent correlation between changes in our estimate of the radial dimension of the magnetotail and intervals when the spacecraft is within or without the magnetopause boundary.

[39] Typical dimensions of the magnetosphere might be 15 and $20-25\ R_E$ at $X = 0$ and $-25\ R_E$, respectively. However, our calculations show that, at its most compressed and deflated, the radial dimension of the magnetotail might be as small as 12 or $13\ R_E$ at $X \approx -25\ R_E$; at the same time, section 2.5 shows that the magnetospheric radius near $X \approx 0$ is $8\ R_E$ or less. We note in passing that the increase in radial dimension by approximately $4-5\ R_E$ in $25\ R_E$ of down-tail distance is consistent with our estimate of the magnetotail flaring angle of ~11° (i.e., radius at $X \approx -25\ R_E$ is approximately $8 + 25 \tan 11°\ R_E$).

[40] In the next section we turn to a comparison between our estimate R_{tail} and that of the Shue model. However, before this, we briefly examine our assumption that the amount of flux in the lobe at the location of IMP-8 is equal to the flux through the polar cap, or in other words, that no open flux crosses the tail magnetopause sunwards of IMP-8. This is certainly true when no dayside reconnection has occurred in the recent past. However, if reconnection is ongoing, then newly opened flux tubes will take some time to propagate from the reconnection site into the tail, carried by the flow of the magnetosheath. At a solar wind speed of 600 km s^{-1}, propagation from the sub-solar magnetopause to IMP-8 (approximately $35\ R_E$) will take 5 or 6 min. If the reconnection rate is 100 kV, then this represents 3.5×10^7 Wb of open flux crossing the magnetopause sunwards of IMP-8, which can be a sizable fraction (~10%) of the open flux in the magnetosphere. In other words, the size of the magnetotail will lag behind changes observed in the polar cap area but only by a few minutes. Consequently, on the timescales involved in the present study we can assume that flux is transported almost instantly to the location of IMP-8. In section 3.4 we will use a variation of this argument to determine the instantaneous length of the magnetotail.

3.3. Comparison With *Shue et al.* [1998]

[41] The model of *Shue et al.* [1998] is based upon observations of magnetopause crossings by many spacecraft over a broad range of X. These have been correlated with

upstream measurements of $P_{\rm dyn}$ and IMF B_z to give an empirically determined formula for the shape of the magnetopause. The model derives two main quantities from P_{dyn} and B_z which in turn determine the shape of the magnetopause. These are r_0, the subsolar stand-off distance, and α, which determines the flaring of the magnetosphere. The first term recognizes that enhanced solar wind dynamic pressure compresses the magnetosphere, especially on the dayside. The model is not explicitly parameterized by the open flux content of the magnetosphere, as this is difficult to quantify on a routine basis. However, the dependence of the flaring parameter α on B_z implicitly recognizes that the open flux content is on average greater when the IMF is directed southward; hence the magnetotail is inflated and so the degree of flaring is larger than during northwards directed IMF. The effects of varying both $P_{\rm dyn}$ and B_z on the model prediction can be seen in Figure 11e. For instance, when $P_{\rm dyn}$ increases in a stepwise manner at 0655 UT, $R_{\rm Shue}$ decreases markedly. As B_z is also positive at this time, $R_{\rm Shue}$ is especially small. At 0950 UT, when B_z becomes negative, although $P_{\rm dyn}$ does not change significantly at this time, $R_{\rm Shue}$ increases to reflect an expected accumulation of open flux in the magnetotail. However, we know that the quantity of open flux is not so directly linked to the orientation of the IMF, and this parameterization is overly simplistic; the quantity of open flux in the magnetosphere depends crucially on the past history of dayside and nightside reconnection. Thus the magnetosphere does not inflate to the size predicted by $R_{\rm Shue}$ until about 1030 UT and continues to grow beyond this as F_{PC} continues to increase. This can also be seen immediately following the shock arrival, when our prediction $R_{\rm tail}$ steps inward at the pressure increase but then continues to reduce in size as flux is closed by SB2 over the following 30 min or so. The Shue model, then, indicates the size the magnetosphere would have if it contained a "typical" amount of flux for the upstream IMF B_z component, and which is compressed to an average $B_{\rm lobe}$ for the given $P_{\rm dyn}$. At times when the open flux content of the magnetosphere can be considered typical (say 0.6 GWb), the correspondence between $R_{\rm tail}$ and $R_{\rm Shue}$ is good, for example near 0500, 0600, and 1030 UT. If the flux content is greater than or less than this value, however, the magnetosphere can become considerably larger or smaller than predicted. In our case, the Shue model is unable to take into account the combined effect of a simultaneously compressed and deflated tail.

[42] At the subsolar point the Shue model predicts a magnetopause standoff distance of 8 R_E when the magnetosphere is at its most compressed (see Figure 1). Although the magnetotail is considerably more compressed than predicted at this time, this subsolar prediction is certainly consistent with our observation that the magnetopause does not cross geosynchronous orbit at $X = 6.6$ R_E. This is to be expected, as the position of the subsolar magnetopause does not depend on the open flux content of the magnetosphere to the same extent as in the tail. It is known, however, that under extreme southward IMF coupling, the dayside magnetopause can become eroded inwards as closed flux is opened and peeled antisunward to form the magnetotail [e.g., *Aubry et al.*, 1970; *Holzer and Slavin*, 1978]. Conversely, if the open flux content of the magnetosphere is low, then the subsolar standoff distance may even be greater than the Shue prediction. Overall, during our interval, this would result in a relatively pointed and low cross-section magnetosphere.

3.4. Length of the Magnetotail

[43] At the end of section 3.2 we argued that the open flux crossing the magnetopause sunward of IMP-8 was equal to the dayside reconnection rate integrated over the time taken for field lines to be transported from the subsolar point to the spacecraft location. We can use a similar argument to estimate the length of the magnetotail. Previous observations have shown that tail-like features can be observed as far downstream of the Earth as 1000 R_E [e.g., *Cowley*, 1991, and references therein] and perhaps even $\sim$3000 R_E [*Intriligator et al.*, 1979].

[44] The growth and decay of open flux threading the polar cap can be represented by the following expression of Faraday's Law [see *Milan et al.*, 2003, and references therein]:

$$\frac{dF_{PC}(t)}{dt} = \Phi_{\rm day}(t) - \Phi_{\rm night}(t), \tag{4}$$

where $\Phi_{\rm night}$ and $\Phi_{\rm day}$ are the voltages associated with reconnection in the magnetotail and at the low-latitude magnetopause. In other words, the expansion or contraction of the polar cap, as represented in Figure 11a, is controlled by the competition between the instantaneous creation and destruction of open flux. Following reconnection on the dayside, newly opened field lines are carried antisunward by the solar wind flow to form the magnetotail. Some time Δt after reconnection, these field lines cross the magnetopause and enter the solar wind (points C in Figure 1), reducing the overall flux within the magnetotail F, at a down-tail distance of $x = V_{SW}\Delta t$. For simplicity we assume a constant value of V_{SW}, thereby neglecting the interaction between faster and slower elements within the solar wind, and the consequent compression or rarefraction of the magnetic field. By extension of equation (4), and recognizing that $dx = V_{SW}dt$, this can be represented as

$$\frac{dF(x,t)}{dx} = -\frac{1}{V_{SW}}\Phi_{\rm day}(t-\Delta t) = -\frac{1}{V_{SW}}\Phi_{\rm day}\left(t - \frac{x}{V_{SW}}\right). \tag{5}$$

At the earthward end of the tail, $x = 0$, the amount of open flux $F(x = 0, t)$ is just that threading the polar cap, $F_{PC}(t)$. By integration, the flux remaining in the tail at any particular x and t is given by

$$F(x,t) = F_{PC}(t) - \frac{1}{V_{SW}}\int_0^x \Phi_{\rm day}\left(t - \frac{x}{V_{SW}}\right)dx. \tag{6}$$

The tail terminates at $x = L_{\rm tail}$, such that $F(x, t) = 0$, or in other words

$$\int_0^{L_{\rm tail}} \Phi_{\rm day}\left(t - \frac{x}{V_{SW}}\right)dx = V_{SW}F_{PC}(t). \tag{7}$$

Thus the length of the magnetotail, and the profile of open flux within it, can be found from a knowledge of the present size of the polar cap and the past history of dayside reconnection. The former is found from our ionospheric

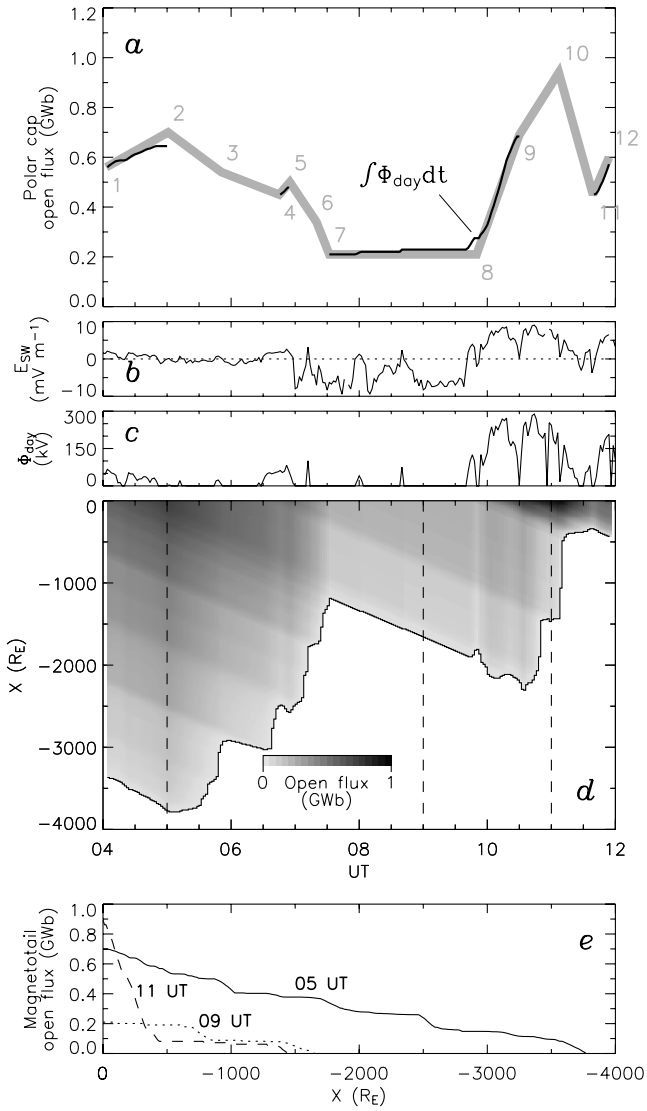

Figure 12. (a) The open flux content of the magnetosphere (grey) reproduced from Figure 11a and compared with predictions of the polar cap growth due to the dayside reconnection rate Φ_{day} (dark line). (b) The solar wind electric field E_{SW}. (c) Predicted dayside reconnection rate Φ_{day}. (d) The flux content and length of the magnetotail. (e) Representative profiles of the flux content of the tail, from 0500, 0900, and 1100 UT (see dashed lines in Figure 12d).

observations and is reproduced in Figure 12a, and the latter we estimate from upstream observations of the solar wind electric field $E_{SW} = -V_{SW}B_z$, presented in Figure 12b. We assume that the dayside reconnection rate (reconnection voltage) can be found by applying this electric field across a constant portion of the dayside magnetopause L_{MP}, and that reconnection only takes place if the IMF is directed southwards, $B_z < 0$, such that

$$\Phi_{\text{day}} = \begin{cases} L_{MP}E_{SW} & B_z < 0 \\ 0 & B_z < 0 \end{cases}, \tag{8}$$

presented in Figure 12c [see also, e.g., *Holzer and Slavin*, 1979]. Then, from equation (4), the rate of expansion of the polar cap should be equal to Φ_{day} when no nightside reconnection is taking place, $\Phi_{\text{night}} = 0$, which should be the case between auroral stages 1–2, 4–5, 7–9, and 11–12, as defined in section 3.1 (see Figures 11a and 12a). At these times we have superimposed the expected growth in F_{PC} from equations (4) and (8); this close match between prediction and observation is found for $L_{MP} = 5\ R_E$ (in good agreement with *Holzer and Slavin* [1979]). We can use this relationship to find Φ_{day} at all times. Then, coupled with our measurements of F_{PC}, and assuming a constant solar wind speed of 600 km s^{-1}, we can use equations (6) and (7) to find the instantaneous length of the magnetotail and the profile of the open flux within it. These are shown in Figure 12d, the grey scale indicating the amount of open flux remaining in each magnetotail lobe as a function of down-tail distance. The point at which the open flux goes to zero is marked by the solid curve.

[45] Our calculations suggest that during the 8 hours presented the magnetotail varies in length between almost 4000 R_E and as little as 400 R_E. Somewhat counter-intuitively, the magnetotail is at its shortest just following the time that the polar cap is at its maximum size. Indeed, the tail shortens dramatically during periods of rapid tail reconnection, that is after each substorm onset. During periods of mild or even zero growth of the polar cap, provided no nightside reconnection occurs, the magnetotail continues to grow in length at the solar wind speed. Three representative profiles of the open flux content of the magnetotail are shown in Figure 12e, from 0500, 0900, and 1100 UT, marked by vertical dashed lines in Figure 12d. At 0500 UT, the polar cap contains a typical amount of open flux, of order 0.6 GWb, and this determines the near-Earth open flux content of the tail. The tail then decreases gradually in open flux along its length, reflecting the fact that over the preceding few hours the dayside reconnection rate has been low and relatively steady (not shown). At 0900 UT, however, the tail is much shorter and contains less open flux, as the polar cap is smaller and nightside reconnection associated with SB2 has recently truncated the tail. Finally, at 1100 UT the polar cap is large and the open flux content of the near-Earth tail mirrors this; however, the flux content drops dramatically in the first 400 R_E of its length as this open flux was all created recently in the polar cap expansion after 1000 UT, and these field lines have not existed for a sufficient time to be stretched to greater lengths. Beyond $X = -400\ R_E$, the remaining open flux is that which predates the last polar cap expansion. This older, extended tail is rapidly being eroded by on-going nightside reconnection associated with SB3; continuing reconnection will see the disappearance of this fossil tail, which indeed occurs after 1115 UT.

[46] We note at this point the caveat that our model shows the length of that portion of the magnetotail which contains open flux. Beyond this point all field lines are entirely disconnected from the Earth. However, as suggested by *Cowley* [1991], there will be a remnant tail which contains recently disconnected field lines that are still highly kinked and stretch back towards the tail reconnection site (D in Figure 1). These field lines will rapidly contract along the length of the tail, though as they do so their down-tail ends continue to move to ever greater distances with the solar wind flow. Thus if the speed of retraction of the field lines is

twice that of the flow of the solar wind, and the tail reconnection site is assumed to be relatively close to the Earth, that is earthward of 100 or 200 R_E, then the overall length of the tail may be several times that of the predicted open flux region.

4. Conclusions

[47] We have demonstrated a direct link between the radial dimension of the magnetotail and the amount of open flux in the magnetosphere. Following a large step in solar wind dynamic pressure, the magnetosphere becomes highly compressed. Coupled with the closure of most of the open flux in the system in response to this compression, we predict that the magnetotail radius at $X \approx -25$ R_E becomes as small as 12 R_E. Despite a gradual slackening of the solar wind pressure, the magnetotail radius does not recover to more typical dimensions until over 3 hours later, approximately 40 min after a southward turning of the IMF. These 40 min are interpreted as the time scale necessary to replenish the magnetosphere with open flux and hence reinflate the magnetotail, through the action of low-latitude magnetopause reconnection.

[48] In addition we find that the magnetic field strength within the magnetotail lobes depends to first order on the upstream solar wind dynamic pressure. This is understood as the compression of the magnetotail to the point that the internal magnetic pressure balances the normal stress exerted by the solar wind flow. The magnetic pressure is found to be approximately one tenth of the solar wind dynamic pressure, reflecting pressure variations within the magnetosheath and the angle of attack of the flow against the flared magnetopause.

[49] Typically, the average location of the polar cap boundary, estimated from the latitude of the auroral oval, suggests that some 7 or 8% of the Earth's magnetic flux is open to the solar wind. During the interval of study, this reduces to just 2.5%, indicating a nearly closed magnetosphere. Despite this, in the subsequent 3 hours the auroral oval assumes a quiescent but typical appearance, with a nightside poleward boundary near a latitude of 70°, suggesting an open polar cap of apparently significant size. This indicates that care must be taken in using auroral observations to determine the amount of open flux in the magnetosphere. On the other hand, with this caveat understood, auroral observations can give important information regarding the large-scale configuration of the magnetosphere and magnetotail. Our study also demonstrates the potential limitations of magnetopause models which assume that the instantaneous open flux content of the magnetosphere depends solely on the immediate upstream solar wind and IMF conditions. Finally, our model of magnetotail length and flux content shows the tail to be a highly dynamic structure, with dramatic changes in open flux content with time and along its length, reflecting the past history of dayside and nightside reconnection.

[50] **Acknowledgments.** SEM and SWHC are supported by PPARC grant PPA/N/S/2000/00197. DMW is supported by PPARC grant PPA/A/S/2001/00344. We would like to thank the following PIs and their respective teams for provision of data discussed in this study: N. F. Ness of the Bartol Research Institute (ACE MFI), D. J. McComas of the Southwest Research Institute (ACE SWE), K. W. Ogilvie of NASA GSFC (Wind SWE), S. Kokubun of STELAB, Nagoya University (Geotail MGF), L. A. Frank of Iowa University (Geotail CPI), C. T. Russell of the University of California, Los Angeles (Polar MFE), and D. Belian of LANL (LANL SOPA). All but the LANL data were provided through the SPDF and CDAWeb at NASA GSFC. Spacecraft locations were provided through the SSC and SSCWeb at NASA GSFC.

[51] Lou-Chuang Lee thanks Steven M. Petrinec and Thomas J. Immel for their assistance in evaluating this paper.

References

Arnoldy, R. L., and K. W. Chan (1969), Particle substorms observed at the geostationary orbit, *J. Geophys. Res.*, *74*, 5019–5028.

Aubry, M. P., C. T. Russell, and M. G. Kivelson (1970), Inward motion of the magnetopause before a substorm, *J. Geophys. Res.*, *75*, 7018–7031.

Baker, D. N., S. J. Bame, R. D. Belian, W. C. Feldman, J. T. Gosling, P. R. Higbie, E. W. Hones Jr., D. J. McComas, and R. D. Zwickl (1984), Correlated dynamical changes in the near-earth and distant magnetotail regions: ISEE 3, *J. Geophys. Res.*, *89*, 3855–3864.

Caan, M. N., R. L. McPherron, and C. T. Russell (1973), Solar wind and substorm-related changes in the lobes of the geomagnetic tail, *J. Geophys. Res.*, *78*, 8087–8096.

Caan, M. N., R. L. McPherron, and C. T. Russell (1975), Substorm and interplanetary magnetic field effects on the geomagnetic tail lobes, *J. Geophys. Res.*, *80*, 191–194.

Chapman, S., and V. C. A. Ferraro (1931), A new theory of magnetic storms, *J. Geophys. Res.*, *36*, 171–186.

Coroniti, F. V., and C. F. Kennel (1972), Changes in magnetospheric configuration during the substorm growth phase, *J. Geophys. Res.*, *77*, 3361–3370.

Cowley, S. W. H. (1991), The structure and length of tail-associated phenomena in the solar wind downstream from the Earth, *Planet. Space Sci.*, *7*, 1039–1043.

Davis, T. N., and M. Sugiura (1966), Auroral electrojet activity index AE and its universal time variations, *J. Geophys. Res.*, *71*, 785–801.

Dungey, J. W. (1961), Interplanetary magnetic fields and the auroral zones, *Phys. Rev. Lett.*, *6*, 47–48.

Dungey, J. W. (1965), The length of the geomagnetic tail, *J. Geophys. Res.*, *70*, 1753.

Fairfield, D. H. (1986), Time variations of the distant magnetotail, *Geophys. Res. Lett.*, *13*, 80–83.

Fairfield, D. H. (1987), Structure of the geomagnetic tail, in *Magnetotail Physics*, edited by A. T. Y. Lui, pp. 23–33, Johns Hopkins Univ. Press, Baltimore, Md.

Frey, H. U., T. J. Immel, G. Lu, J. Bonnell, S. A. Fuselier, S. B. Mende, B. Hubert, N. Ostgaard, and G. Le (2003), Properties of localized, high latitude, dayside aurora, *J. Geophys. Res.*, *108*(A4), 8008, doi:10.1029/2002JA009332.

Fuselier, S. A., H. U. Frey, K. J. Trattner, S. B. Mende, and J. L. Burch (2002), Cusp aurora dependence on interplanetary magnetic field B_z, *J. Geophys. Res.*, *107*(A7), 1111, doi:10.1029/2001JA900165.

Henderson, M. G., J. S. Murphree, and J. M. Weygand (1996), Observations of auroral substorms occurring together with preexisting "quiet time" auroral patterns, *J. Geophys. Res.*, *101*, 24,621–24,640.

Holzer, R. E., and J. A. Slavin (1978), Magnetic flux transfer associated with expansions and contractions of the dayside magnetosphere, *J. Geophys. Res.*, *83*, 3831–3839.

Holzer, R. E., and J. A. Slavin (1979), A correlative study of magnetic flux transfer in the magnetosphere, *J. Geophys. Res.*, *84*, 2573–2578.

Intriligator, D. S., H. R. Collard, J. D. Mihalov, O. L. Vaisberg, and J. H. Wolf (1979), Evidence for Earth magnetospheric tail associated phenomena at 3100 R_E, *Geophys. Res. Lett.*, *6*, 585.

Lockwood, M., S. E. Milan, T. Onsager, C. H. Perry, J. A. Scudder, C. T. Russell, and M. Brittnacher (2001), Cusp ion steps, field-aligned currents and poleward-moving auroral forms, *J. Geophys. Res.*, *106*, 29,555–29,569.

Maezawa, K. (1975), Magnetotail boundary motion associated with geomagnetic substorms, *J. Geophys. Res.*, *80*, 3543–3548.

Matsushita, S. (1967), Geomagnetic disturbances and storms, in *Physics of Geomagnetic Phenomena II*, edited by S. Matsushita and W. H. Campbell, pp. 793–819, Academic, San Diego, Calif.

McIlwain, C. E. (1974), Substorm injection boundaries, in *Magnetospheric Physics*, edited by B. M. McCormac, p. 143, D. Reidel, Norwell, Mass.

Mead, G. D., and D. B. Beard (1964), Shape of the geomagnetic field-solar wind boundary, *J. Geophys. Res.*, *69*, 1169–1179.

Milan, S. E., M. Lester, S. W. H. Cowley, and M. Brittnacher (2000a), Dayside convection and auroral morphology during an interval of northward interplanetary magnetic field, *Ann. Geophys.*, *18*, 436–444.

Milan, S. E., M. Lester, S. W. H. Cowley, and M. Brittnacher (2000b), The convection and auroral response to a southward turning of the IMF:

POLAR UVI, CUTLASS, and IMAGE signatures of transient magnetic flux transfer at the magnetopause, *J. Geophys. Res.*, *105*, 15,741–15,756.

Milan, S. E., M. Lester, S. W. H. Cowley, K. Oksavik, M. Brittnacher, R. A. Greenwald, G. Sofko, and J.-P. Villain (2003), Variations in polar cap area during two substorm cycles, *Ann. Geophys.*, *21*, 1121–1140.

Ness, N. F. (1987), Magnetotail research: the early years, in *Magnetotail Physics*, edited by A. T. Y. Lui, pp. 11–20, Johns Hopkins Univ. Press, Baltimore, Md.

Petrinec, S. M., and C. T. Russell (1996), Near-Earth magnetotail shape and size as determined from the magnetopause flaring angle, *J. Geophys. Res.*, *101*, 137–152.

Russell, C. T., and R. L. McPherron (1973), The magnetotail and substorms, *Space Sci. Rev.*, *15*, 205–266.

Sauvaud, J. A., and J. R. Winckler (1980), Dynamics of plasma, energetic particles, and fields near synchronous orbit in the nighttime sector during magnetospheric substorms, *J. Geophys. Res.*, *85*, 2043–2056.

Shue, J.-H., et al. (1998), Magnetopause location under extreme solar wind conditions, *J. Geophys. Res.*, *103*, 17,691–17,700.

Slavin, J. A., E. J. Smith, D. G. Sibeck, D. N. Baker, R. D. Zwickl, and S.-I. Akasofu (1985), An ISEE 3 study of average and substorm conditions in the distant magnetotail, *J. Geophys. Res.*, *90*, 10,875–10,895.

Torr, M. R., et al. (1995), A far ultraviolet imager for the international solar-terrestrial physics mission, *Space Sci. Rev.*, *71*, 329–383.

Tsyganenko, N. A. (1995), Modeling the Earth's magnetospheric magnetic field confined within a realistic magnetopause, *J. Geophys. Res.*, *100*, 5599–5612.

Unti, T., and G. Atkinson (1968), Two-dimensional Chapman-Ferraro problem with neutral sheet: 1. The boundary, *J. Geophys. Res.*, *73*, 2319–2327.

Zhang, Y., L. J. Paxton, T. J. Immel, H. U. Frey, and S. B. Mende (2003), Sudden solar wind dynamic pressure enhancements and dayside detached auroras: IMAGE and DMSP observations, *J. Geophys. Res.*, *108*(A4), 8001, doi:10.1029/2002JA009355.

C. W. Carlson and M. Fillingim, Space Science Laboratory, University of California, Berkeley, CA 94720, USA. (cwc@ssl.berkeley.edu; matt@ssl.berkeley.edu)

S. W. H. Cowley, M. Lester, S. E. Milan, and D. M. Wright, Department of Physics and Astronomy, University of Leicester, Leicester LE1 7RH, UK. (s.cowley@ion.le.ac.uk; m.lester@ion.le.ac.uk; steve.milan@ion.le.ac.uk; d.wright@ion.le.ac.uk)

H. J. Singer, Space Environment Center, Boulder, CO 80303, USA. (howard.singer@noaa.gov)

J. A. Slavin, NASA Goddard Space Flight Center, Greenbelt, MD 20771, USA. (jim.slavin@gsfc.nasa.gov)